Scour depth in confluences considering tributary flow, bank slope, and post-confluence conditions

Payam Khosravinia, Amir Malekpour, Mohammad Reza Nikpour and Ali Hosseinzadeh Dalir

ABSTRACT

In this paper, scouring in confluences was experimentally studied considering the effects of bank slope angle (θ) of the main channel, discharge ratio (Q_r) of tributary channel and densimetric Froude number (Fr_{g3}) of the post-confluence channel. The experiments were conducted using a constant confluence angle (α) equal to 90°, various bank slope angles of 45°, 60°, 75° and 90°. Applying different Q_r and Fr_{g3}, the maximum effect of θ on scour depth was observed when the minor Q_r was used in the tributary channel. The mildest bank slope angle caused the minimum scour depth for any given Fr_{g3}. Generally, the experiment using $\theta = 45°$ and $Q_r = 0.194$ showed the best performance and reduced the maximum scour depth by 46%. Considering two obtained empirical relationships, it was concluded that the effect of θ on the height of the point bar is more than its effect on the scour depth. Finally, Fr_{g3} and θ demonstrated their greatest influences on dimensionless scour depth (d_{se}/y_3) and dimensionless height of point bar (H_{se}/B_3), respectively.

Key words | channel bank slope, densimetric Froude number, discharge ratio, point bar

Payam Khosravinia
Dept. of Water Engineering,
University of Kurdistan,
Sanandaj,
Iran

Amir Malekpour (corresponding author)
University of Guilan,
Rasht,
Iran
E-mail: *malekpour@guilan.ac.ir*

Mohammad Reza Nikpour
Water Eng. Dept.,
University of Mohaghegh Ardabili,
Ardabil,
Iran

Ali Hosseinzadeh Dalir
Dept of Water Eng.,
University of Tabriz,
Tabriz,
Iran

HIGHLIGHTS

- The effect of geometry of channel and flow condition at the confluence on scouring and point bars.
- Presenting experimental relationships to estimate the scour depth and the height of point bar.

NOMENCLATURE

d_{se}	Scour depth
H_{se}	Height of sediment bar
Fr_{g3}	Densimetric Froude number at the post-confluence channel
G_s	Specific density of sediment particles
α	Confluence angle
Q_r	Discharge ratio
V_c	Critical velocity
u_{*c}	Critical shear velocity
ρ_s	Density of sediment particles
Q_b	Bed load
B	Bottom width of channel
ρ	Water density
g	Gravitational acceleration
σ	Surface tension
μ	Dynamic viscosity
θ	Bank slope angle of the main channel
S_0	Longitudinal bed slope of the main channel at the confluence
Q_1	Discharge at the upstream channel
Q_2	Discharge at the tributary channel
Q_3	Discharge at the post-confluence channels

doi: 10.2166/ws.2020.131

V_3 Velocity at the post-confluence channel
y_1 Flow depth at the upstream channel
y_2 Flow depth at the tributary channel
y_3 Flow depth at the post-confluence channel
R_e Reynolds number
W_e Weber number

INTRODUCTION

Scouring and sediment deposition are important challenges within rivers and natural channels because of their negative impacts on the performance of hydraulic structures. For example, the design embedment depth of bridge piers can be affected by scouring. In a confluence where a tributary flow joins a main channel, the formation of recirculating vortex flow and increased velocity cause scouring and subsequently sediment deposition along the post-confluence channel (Mosley 1976; Rhoads & Kenworthy 1998).

The flow pattern in a confluence is complex and influenced by many factors, some of which have been reported in the literature including the ratio of tributary flow to the main flow, hereafter referred to as *discharge ratio*, and the rate of momentum transfer between the main stream and the tributary channel (Biron *et al.* 2002; Boyer *et al.* 2006). Best (1987) illustrated the flow pattern in a confluence, as shown in Figure 1.

According to Figure 1, six regions can be identified within the confluence hydrodynamic zone including (1) a stagnation region at the upstream corner of the confluence, (2) a flow deflection region at the junction point, (3) a separation region next to the downstream corner of the confluence, (4) a maximum velocity region in the main channel due to flow contraction (less flow width) caused by the formation of a separation zone, (5) a flow recovery zone downstream of the maximum velocity region at the post-confluence channel, and (6) a shear layer developed between the two combining flows. Expansion of stagnation and separation regions results in the enlargement of sediment bars (Best 1987). According to previous studies (Rhoads & Sukhodolov 2008; Shakibainia *et al.* 2010; Nazari-Giglou *et al.* 2016; Yuan *et al.* 2017), two factors intensify the bed-shear stress in a confluence including, first, the combination of main and tributary flows at the junction point and, second, the strong vortices, helical motions and the kinetic energy. In the literature, several studies have been reported on the flow pattern and sediment transport in confluences. A study by Best & Reid (1984) showed that increasing the confluence angle from 15° to 90° increases the near-bottom velocity by a factor of 1.3. Best (1987) concluded that a confluence angle of 15° causes negligible scouring, whereas greater confluence angles dramatically increase the maximum scour depth. The effect of confluence angle on the formation of sediment bars, i.e. point bars, in post-confluence channels was studied later by Best (1988). The results showed that point bars grow in size when greater confluence angles and discharge ratios are adopted in the experiments.

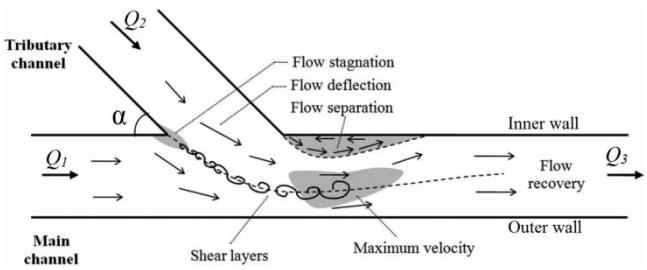

Figure 1 | Flow pattern in a confluence, slightly modified from Best (1987) by Nazari-Giglou *et al.* (2016).

A comprehensive study by Roy *et al.* (1988) on 30 confluences located within a watershed indicated that the flow capacity declined at most of the post-confluence channels. Hager (1989) studied the flow regime in confluences and stated that a minimum discharge ratio of 15% is required for transition from subcritical to supercritical flow. Bryan & Kuhn (2002) experimentally studied the effects of symmetrical and asymmetrical confluences on the flow pattern. It was found that symmetrical confluences create a symmetrical scour pattern mirroring the original channel, whereas asymmetrical confluences cause a symmetrical scour pattern with a confluence angle greater than the original one. The scour pattern considering different confluence angles including 60°, 75° and 90° was experimentally studied by Ghobadian & Shafai-Bajestan (2007). In this regard, Equations (1) and (2) were presented for approximating the maximum scour depth (d_{se}) and the height of the sediment bar at the post-confluence stream (H_{se}),

respectively:

$$\frac{d_{se}}{y_3} = 0.029\ Q_r^{0.73}\ \ Fr_{g3}^{2.03}\ \ \alpha^{0.35} \tag{1}$$

$$\frac{H_{se}}{y_3} = 0.27\ Q_r^{0.638} - 0.559\ Fr_{g3}^{0.321} + 0.21\ \ln\ (\alpha) \tag{2}$$

In addition, Fr_{g3}=densimetric Froude number at the post-confluence channel, as defined in Equation (3), Q_r = discharge ratio, y_3 = flow depth at the post-confluence channel, and α = confluence angle:

$$Fr_{g3} = \frac{V_3}{\sqrt{g(G_s - 1)\, d_{50}}} \tag{3}$$

In Equation (3), V_3 = flow velocity at the post-confluence channel, G_s = specific density of sediment particles (equal to 2.63 in the present study), and d_{50} = median sediment size. Borghei & Jabbari-Sahebari (2010) experimentally investigated the temporal scour pattern in a river confluence with different confluence angles. It was concluded that the position of maximum scour depth moves to the outer wall with time. Meanwhile, Equation (4) was presented for estimating the maximum scour depth:

$$\frac{d_{se}}{y_3} = \frac{2.094}{B_r^{0.461}}\ (\sin\alpha)^{2.393}\ Q_r^{0.338}\ (V_3/V_c)^{1.237} \tag{4}$$

B_r = ratio of the tributary channel width to the main channel width, and V_c = critical velocity, which is approximated using Equation (5):

$$\frac{V_c}{u_{*c}} = 5.75\ \log\ \left(5.53\ \frac{y_3}{d_{50}}\right) \tag{5}$$

where u_{*c} = critical shear velocity. According to Melville & Sutherland (1988), V/V_c must be less than unity to guarantee the clear-water scouring. In addition, V/V_c must be greater than a threshold value, typically $V/V_c > 0.5$, for the onset of scouring.

The study of three-dimensional flow velocity in a 90-degree confluence considering the effect of discharge ratio on the flow pattern showed that an increase in the discharge ratio causes a gradual decrease of the time-averaged velocity at the upstream of the confluence (Liu *et al.* 2012).

Considering the local scouring in curved-edge confluences, it was shown that the increased radius of curvature at a junction point leads to a reduction of maximum scour depth and displacement of its location towards the downstream and center of the main channel (Mohamadi *et al.* 2013). The effect of a main channel with an inclined bank on the amount of suspended sediment load entering an intake was investigated by Seyedian *et al.* (2014). According to the observations, having an inclined bank, the flow was mostly diverted from the surface in a way that the volume of suspended sediment load inside the intake channel was decreased. In the above-mentioned study by Nazari-Giglou *et al.* (2016), the effects of different factors including Froude number, confluence angle, discharge ratio and width ratio on scouring in confluences were additionally investigated, and a formulation for the incipient motion of sediment particles was presented. To reduce scouring in confluences, some studies have focused on presenting countermeasures. For example, Wuppukodur & Chandra (2017) used vanes and circular piles in a 90-degree confluence and Amini *et al.* (2017) applied collars in a 60-degree confluence to reduce the scour depth. There are also many reports on the application of numerical methods for modeling the flow pattern in channel confluences (Hsu *et al.* 1998; Weber *et al.* 2001; Biron *et al.* 2004; Zhang *et al.* 2009; Shakibainia *et al.* 2010; Sharifipour *et al.* 2015; Geberemariam 2016). Debnath *et al.* (2019) in a field study considered the hydrological and morphological characteristics of two rivers at the confluence point. They found that the steeper tributary river enhances the transportation of medium-sized grains to the main river which leads to aggradation and decreased velocity in the downstream.

A comprehensive review of literature shows that the experimental studies conducted on scouring in confluences have mostly focused on the effect of confluence angle and main channels with rectangular cross-sections, whereas natural channels and rivers usually have inclined banks. Considering the inclined river banks in a previous study, Khosravinia *et al.* (2019) investigated the penetration length of the scour hole in different directions at the confluence. The simultaneous effects of river bank slope, post-confluence flow condition and discharge ratio on the

scour depth and sediment bar in a confluence have not been investigated so far, but are experimentally investigated as the first contribution of the current study. Finally, as the second contribution, two equations are presented for estimating the scour depth and the height of the sediment bar at a confluence considering the river bank slope angle, densimetric Froude number of the post-confluence channel and discharge ratio.

DIMENSIONAL ANALYSIS

In order to accomplish the dimensional analysis, different variables that are likely effective on scouring at a confluence must be taken into account, herein presented as Equation (6):

$$f(d_{se}, H_{se}, d_{50}, \rho_s, Q_b, B_1, B_2, B_3, Q_1, Q_2, Q_3, y_1, y_2, y_3, \rho, g, \sigma, \mu, \alpha, \theta, S_0) = 0 \quad (6)$$

where ρ_s = density of sediment particles, Q_b = bed load, B = bottom width of channel, Q = flow discharge, ρ = water density, g = gravitational acceleration, σ = surface tension, μ = dynamic viscosity, θ = bank slope angle of main channel, and S_0 = longitudinal bed slope of main channel at the confluence. The subscripts 1, 2 and 3 refer to the upstream, tributary and post-confluence channels, respectively. The result of dimensional analysis on the scouring at a confluence using Buckingham's π theorem is presented as Equation (7):

$$\frac{d_{se}}{y_3}, \frac{H_{se}}{y_3} = f\left(\frac{Q_2}{Q_3}, \frac{Q_b}{Q_3}, \frac{B_2}{B_3}, \alpha, \theta, S_0, R_{e3}, W_{e3}, Fr_{g3}\right) \quad (7)$$

where R_e and W_e are Reynolds number and Weber number, respectively. Since the effects of viscosity and surface tension were negligible in the experiments, Reynolds and Weber numbers were not considered in the current study. Additionally, bed load transport was not allowed at the upstream of the confluence, so Q_b was eliminated from Equation (7). According to Gurram *et al.* (1997), the bed slope has a negligible effect on the flow pattern in confluences under subcritical flow conditions. Since all experiments were carried out under subcritical condition, S_0 was not considered in the present study. Moreover, the experiments were conducted using a constant confluence angle, i.e. 90-degree confluence. So, Equation (7) can be simplified as Equation (8):

$$\frac{d_{se}}{y_3}, \frac{H_{se}}{y_3} = f\left(\frac{Q_2}{Q_3}, \theta, Fr_{g3}\right) \quad (8)$$

LABORATORY SETUP

In this study, 64 experiments were conducted in a main flume 6 m long, 80 cm wide and 50 cm high. A tributary flume 5 m long, 24 cm wide and 50 cm high was connected perpendicularly, i.e. with a 90-degree confluence angle, to the main flume. The longitudinal bed slopes of the two flumes were set to zero and the false floors and sand beds were used inside them. The false floors made by wooden pieces were installed at a distance of 14 cm over the flume bottom. Meanwhile, the sand was used to fill up the space between the false floors. In order to study the effect of a bank slope on scouring at a confluence, the sloping walls were used in the main flume with different inclination angles, i.e. 45°, 60°, 75° and 90° (section A-A in Figure 2).

The total discharge entering the laboratory setup was adjusted to 25 L/s for all experiments. A calibrated rectangular weir located at the downstream end of the main flume was used to measure the flow discharge. Table 1 presents the discharge values of the three channels joined at the confluence in the current study. To adjust the flow discharge, first, the flow was adjusted in the main channel while the

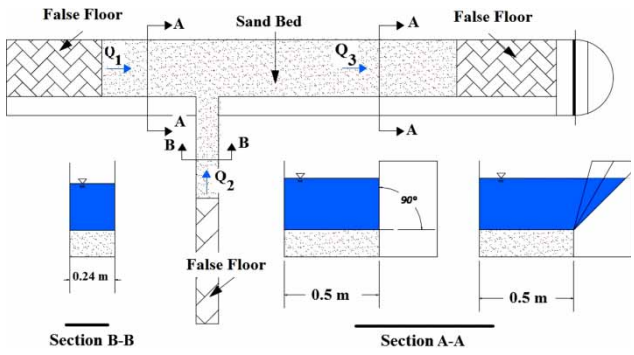

Figure 2 | Schematic view of experimental setup.

Table 1 | Discharge values in three channels joined at the confluence

Q_1 (m³/s)	Q_2 (m³/s)	Q_3 (m³/s)
0.0202	0.0048	0.0250
0.0181	0.0069	0.0250
0.0150	0.0100	0.0250
0.0112	0.0138	0.0250

outlet gate of the tributary channel was closed. Then, the gate of the tributary channel, located at the junction point, was gradually opened in order to establish the designed tributary flow. A number of stop logs were used at the downstream end of the main channel to adjust the tail water depth in the range of 0.152–0.235 m by which the densimetric Froude number was adjusted in the desirable range of 1.28–2.58 (Table 2). Moreover, an ultrasonic gauge (with an accuracy of ±0.1 mm) was applied to measure the water surface elevation. At the entrances of both main and tributary channels, two flow straighteners were applied to prevent excessive turbulence.

In the experiments, uniform sands were used as the sediment material featuring $d_{50} = 1.28$ mm and standard deviation (σ_{std}) = 1.32 mm. Table 2 lists the ranges of the three dimensionless parameters presented in Equation (8), which were used in the experiments in order to evaluate the simultaneous effects of discharge ratio, post-confluence flow condition, and river bank slope on scouring in a confluence.

According to Table 2, four bank slope angles and four discharge ratios were used in the current study. In addition, for each discharge ratio, four values of Froude number and densimetric Froude number were applied by controlling the flow depth in the laboratory setup.

The end of each experiment was reached when the equilibrium condition was established in the scour hole. In the preliminary tests, the longest equilibrium time was obtained for $\theta = 45°$. So, a series of experiments were conducted for $\theta = 45°$ within 72 hours to ensure that the equilibrium condition was reached. For both the maximum and minimum discharge ratios, almost 90 percent of the maximum scour depth was obtained in less than six hours. As a result, all the experiments were continued up to six hours. Then, the flume was carefully depleted of the water without disturbing the sediment bed; and subsequently the dimensions of the scour hole and the height of the sediment bar were measured using a graded rod. In Figure 3, the formation of scouring and a point bar is demonstrated in the laboratory setup for two inclination angles of 45° and 60°. Finally, the multivariate regression method using the statistical software SPSS-15 was applied to find the dimensionless empirical relationships for the maximum scour depth and the height of the point bar in terms of the above-mentioned parameters (Table 2).

Table 2 | Dimensionless parameters used in the current study

Dimensionless parameter	Value/range
Θ	45°, 60°, 75°, 90°
$Q_r = Q_2/Q_3$	0.194, 0.276, 0.400, 0.552
Fr_{g3}	1.28–2.58

RESULTS AND DISCUSSION

A couple of vortices were observed in the beginning of each experiment at the confluence and moved in opposite directions, which triggered scouring of bed materials. Meanwhile, the high velocity due to the flow contraction at the confluence (Figure 1) resulted in transportation of scoured bed materials and formed a point bar in the post-confluence channel (Figure 3), where the velocity decreased due to restoration, i.e. enlargement, of the cross-section. In the

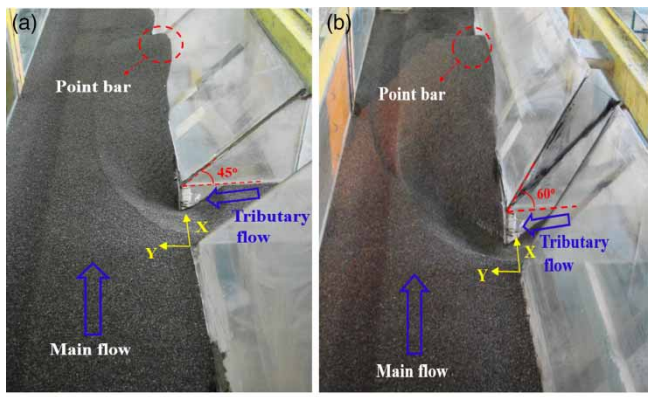

Figure 3 | Scouring and formation of point bar in the laboratory setup.

following sections, a number of graphs are provided for approximation of the maximum scour depth and the height of the point bar. In addition, two empirical equations are presented considering the bank slope of the main channel, the discharge ratio of the tributary channel, and the densimetric Froude number of the post-confluence channel.

Maximum scour depth

Figure 4 shows the variations of dimensionless maximum scour depth (d_{se}/y_3) against densimetric Froude number (Fr_{g3}). According to the results, although d_{se}/y_3 increased with Fr_{g3} for all discharge ratios, the highest rate of increase in d_{se}/y_3 was obtained for the greatest discharge ratio (Q_r), as shown in Figure 4(d).

This result is in agreement with those presented by Ghobadian & Shafai-bajestan (2007) and Amini *et al.* (2017) for main channels with rectangular cross-sections. Comparing Figure 4(a)–4(d), it was observed for given Fr_{g3} and bank slope angle (θ) that increase of discharge ratio resulted in a deeper scour hole, i.e. greater d_{se}/y_3. It conforms to a result by Weber *et al.* (2001) that emphasizes the role of increased discharge ratio in the expansion of the separation zone at a confluence leading to higher velocity, bed shear stress, and consequently deeper scour holes. On the other hand, the mildest bank slope angle ($\theta = 45°$) caused the least d_{se}/y_3 among all the experiments. It can be attributed to the maximum passage of tributary flow over the inclined bank of the post-confluence channel for $\theta = 45°$, which resulted in minor flow contact with the bed materials and minimum scouring. It was also observed

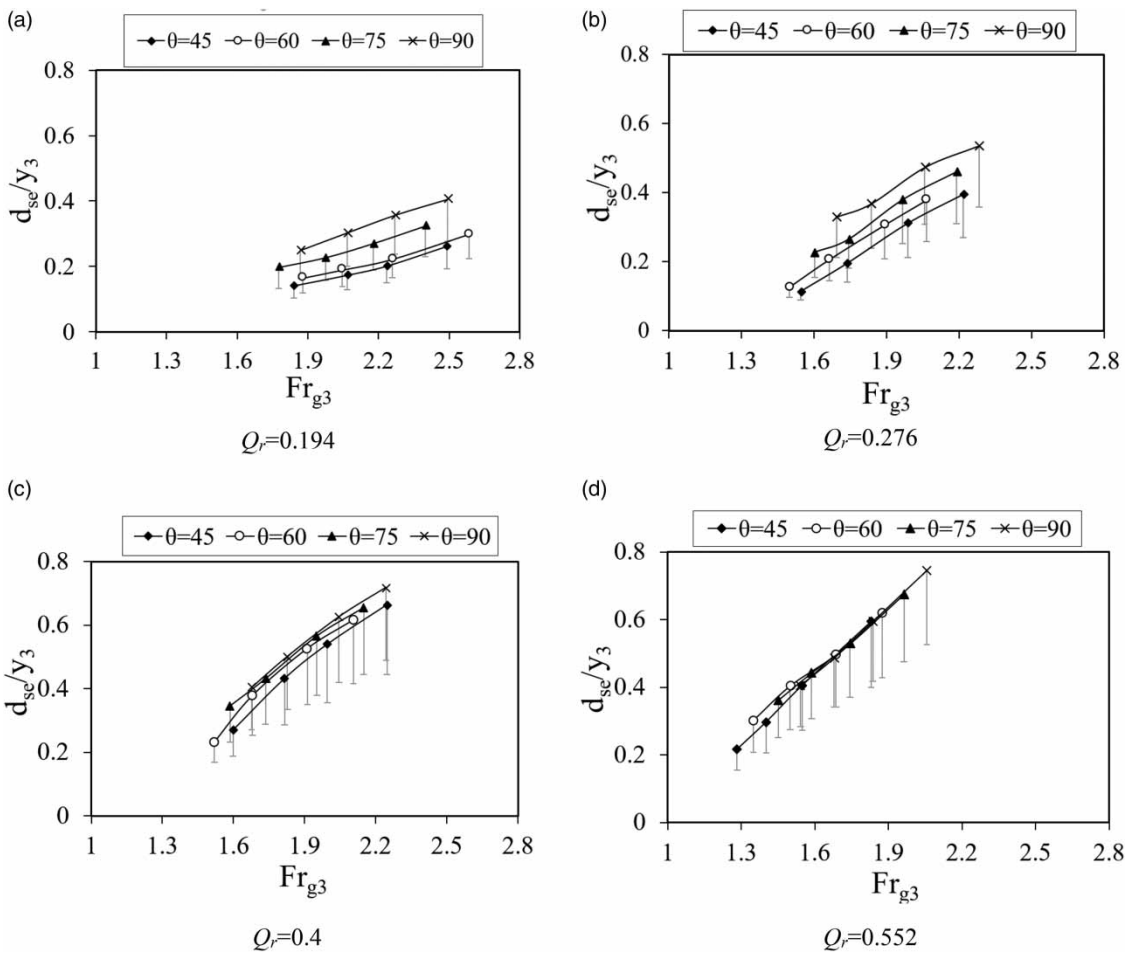

Figure 4 | Variations of dimensionless maximum scour depth versus densimetric Froude number.

that the effect of bank slope angle on the scour depth dramatically fades when Q_r is increased. In other words, the bank slope angle of a river affects the scouring when a modest discharge ratio is established at a confluence.

It is often perceived that tributary flows entering a large river are significantly less than the main flow. Therefore, according to the last paragraph, the effect of river bank slope on the scour depth in a confluence cannot be neglected in practice, as shown in Figure 4(a).

Finally, Equation (9) was derived using the multivariate regression method (with $R^2 = 0.83$) for approximation of the dimensionless maximum scour depth (d_{se}/y_3):

$$\frac{d_{se}}{y_3} = 0.121\, Q_r^{1.104}\, Fr_{g3}^{2.208}\, (\sin\theta)^{0.451} \quad (9)$$

Although the bank slope angle (θ) is effective on the scour depth, comparing the exponents of three variables on the right-hand side of Equation (9), it is concluded that the effect of θ on the maximum scour depth is less than that of the densimetric Froude number (Fr_{g3}) and discharge ratio (Q_r). Additionally, the error bars in Figure 4 indicate that the scour depth is slightly underestimated for lower densimetric Froude numbers. The error increases with increase of both the densimetric Froude number and the bank slope angle.

Figure 5 shows a scatter plot for the dimensionless maximum scour depth of the current study (Equation (9)) compared with Equation (1) by Ghobadian & Shafai-Bajestan (2007) and Equation (4) by Borghei & Jabbari-Sahebari (2010). Neglecting the effect of different river bank slopes, the mentioned previous studies considered the effect of different confluence angles with a constant bank slope ($\theta = 90^\circ$). Therefore, to be able to compare and validate the results of the current study, Equation (9) using $\theta = 90^\circ$ was plotted against Equations (1) and (4) using the confluence angle (α) $= 90^\circ$.

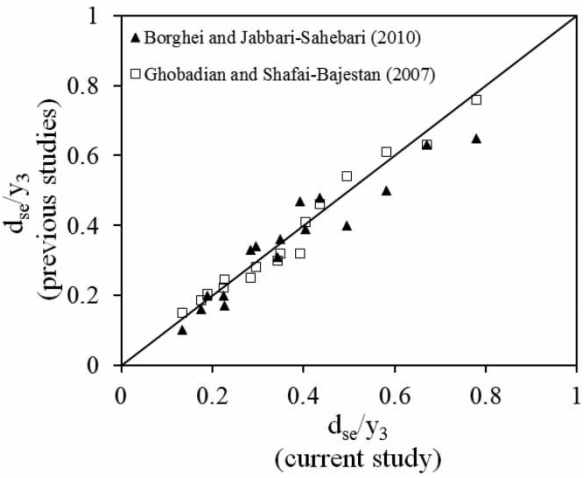

Figure 5 | Dimensionless maximum scour depth in the current study compared with previous studies.

Using the above-mentioned values for α and θ, it is implied that Equation (9) offers close results to Equations (1) and (4). In other words, incorporating the same assumptions as Ghobadian & Shafai-Bajestan (2007) and Borghei & Jabbari-Sahebari (2010), Equation (9) can generate similar results while having the advantage of taking into account the river bank slope.

Maximum height of point bar

In the early stages of each experiment, a point bar formed and gradually moved to the downstream. It became flatter when greater discharge ratios were established in the tributary channel, whereas the reduction of discharge ratio and densimetric Froude number caused sharper point bars. This result is similar to that of Gong *et al.* (2011) emphasizing the role of decreased tributary flows from Yangtze to Wangyu in creating higher and sharper point bars in some cross-sections. Moreover, neglecting the effect of river bank slope, Biron *et al.* (2002) claimed that the increase of discharge ratio and densimetric Froude number leads to the displacement of a point bar toward the downstream of the post-confluence channel.

In Figure 6, the maximum dimensionless height of the point bar in a confluence (H_{se}/y_3) was plotted against densimetric Froude number considering different discharge ratios and bank slope angles of a river. It is obvious that the highest point bars formed in the post-confluence channel belong to the experiments with $\theta = 90^\circ$. Increasing the discharge ratio to $Q_r = 0.552$, the experiments with $\theta = 75^\circ$ generated close results to those with $\theta = 90^\circ$.

Additionally, with increase of θ, an average increase of H_{se}/y_3 by 41.7%, 29.4%, 27.8%, and 23.4% was obtained for $Q_r = 0.194$, 0.276, 0.4, and 0.552, respectively. Similar to the previous section, an empirical relationship was

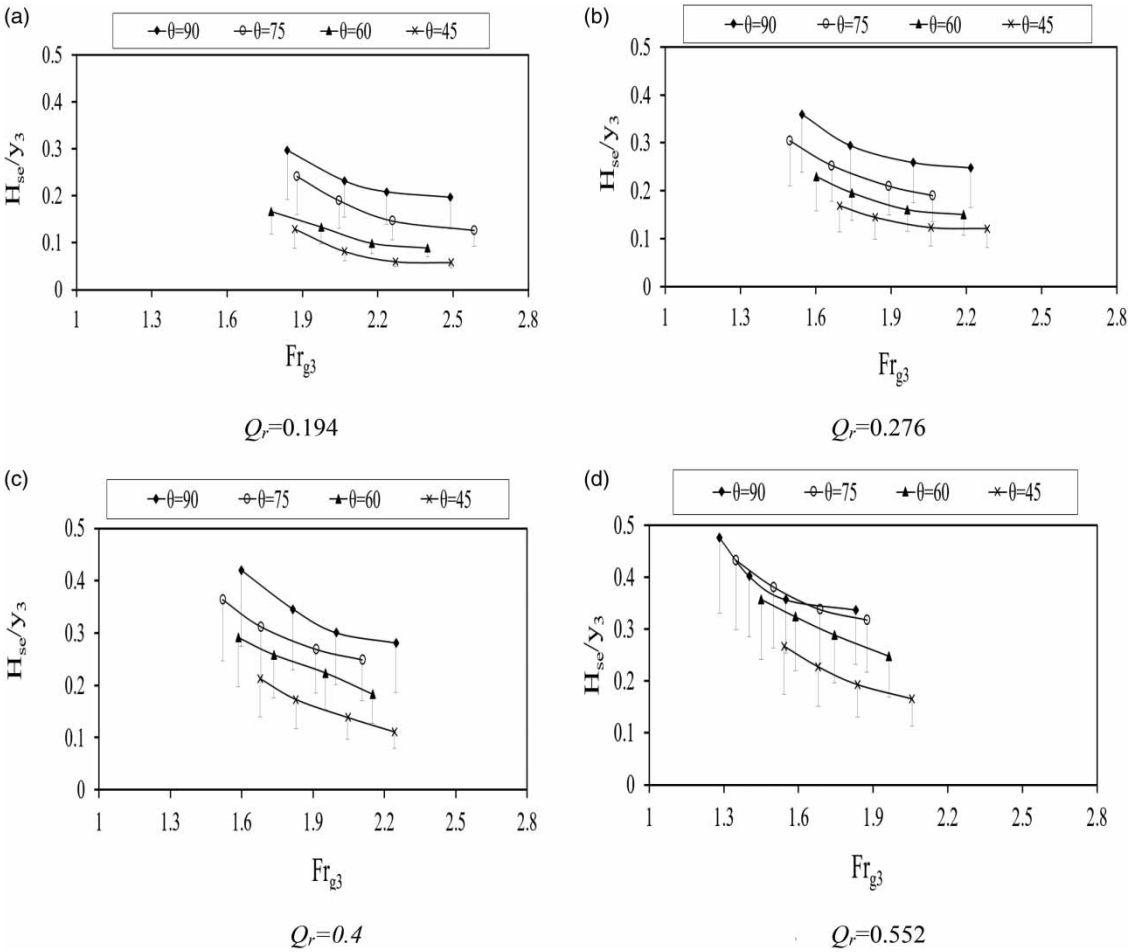

Figure 6 | Maximum dimensionless height of point bar against densimetric Froude number for different bank slope angles and discharge ratios.

derived for approximating the maximum height of the point bar using a multivariate regression method with $R^2 = 0.8$ (Equation (10)):

$$\frac{H_{se}}{B_3} = 0.296\, Q_r^{0.359}\; Fr_{g3}^{-1.046}\; (\sin\theta)^{1.782} \tag{10}$$

Considering the exponents on the right-hand side of Equation (10), the prevailing effect of bank slope on the maximum dimensionless height of the point bar is implied, as opposed to its effect on dimensionless maximum scour depth (Equation (9)). It is also interesting to note that greater discharge ratio (Q_r) and bank slope angle (θ) cause higher point bars, whereas greater densimetric Froude numbers (Fr_{g3}) reduce the maximum height of point bar in the post-confluence channel. The error bars in Figure 6 demonstrate that less error occurs for higher densimetric Froude numbers, as opposed to the error bars in Figure 4. Moreover, the increase in bank slope angle leads to higher errors in estimation of the height of the point bar, similar to Figure 4.

Figure 7 demonstrates the scatter plot of the obtained dimensionless heights of the point bar in the current study (Equation (10)) against those calculated using Equation (2) (Ghobadian & Shafai-Bajestan (2007)) for a main channel with rectangular cross-section and the confluence angle (α) = 90°. It is aimed at validating Equation (10) via using the inputs and assumptions of Equation (2) as a benchmark relationship. Applying the same assumptions, it is obvious that Equation (10) appropriately generates close results to Ghobadian & Shafai-Bajestan (2007).

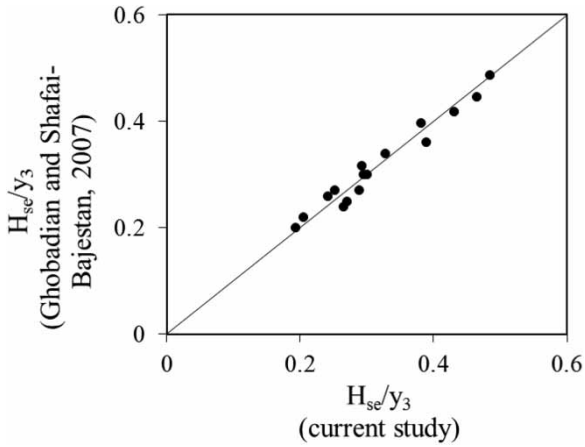

Figure 7 | Dimensionless height of point bar in current study for bank slope angle of 90° compared with the previous study by Ghobadian & Shafai-Bajestan (2007).

With increase of Fr_{g3}, the maximum height of the point bar generally emerged farther from the confluence in the downstream direction. For different values of Q_r and θ, the locations of four maximum point bars corresponding to four Fr_{g3} values (referring to Table 1) are shown in Figure 8. The directions of the X and Y axes were specified earlier in Figure 3. Moreover, the upstream corner of the confluence was adopted as the origin of the X–Y coordinate system. In Figure 8, the negative Y/B_3 implies that the maximum point bar is located on the inclined bank.

It is evident that point bars were created on the sloping bank in the cases of milder inclination angles ($\theta = 45°$ and 60°). Meanwhile, when minor discharge ratios ($Q_r = 0.194$ and 0.276) were used (Figure 8(a) and 8(b)), the point bars were formed at greater distances from the confluence for $\theta = 45°$ and 60°. Contrariwise, when minor discharge ratios were used in the laboratory flume for the cases of $\theta = 75°$ and 90° (Figure 8(c) and 8(d)), the point bars emerged close to the confluence. But the gradual increase of discharge ratio could displace the point bars again to farther locations in the downstream direction. Shakibainia *et al.* (2010) stated that the formation of a point bar close to the inner wall of the post-confluence channel is due to the reduced pressure in the flow separation zone. In the current study, the observations demonstrated that point bars were created at greater distance from the beginning of the post-confluence channel when θ was decreased. Therefore, for milder bank slope angles, there seems to be a smaller separation zone immediately downstream of confluence

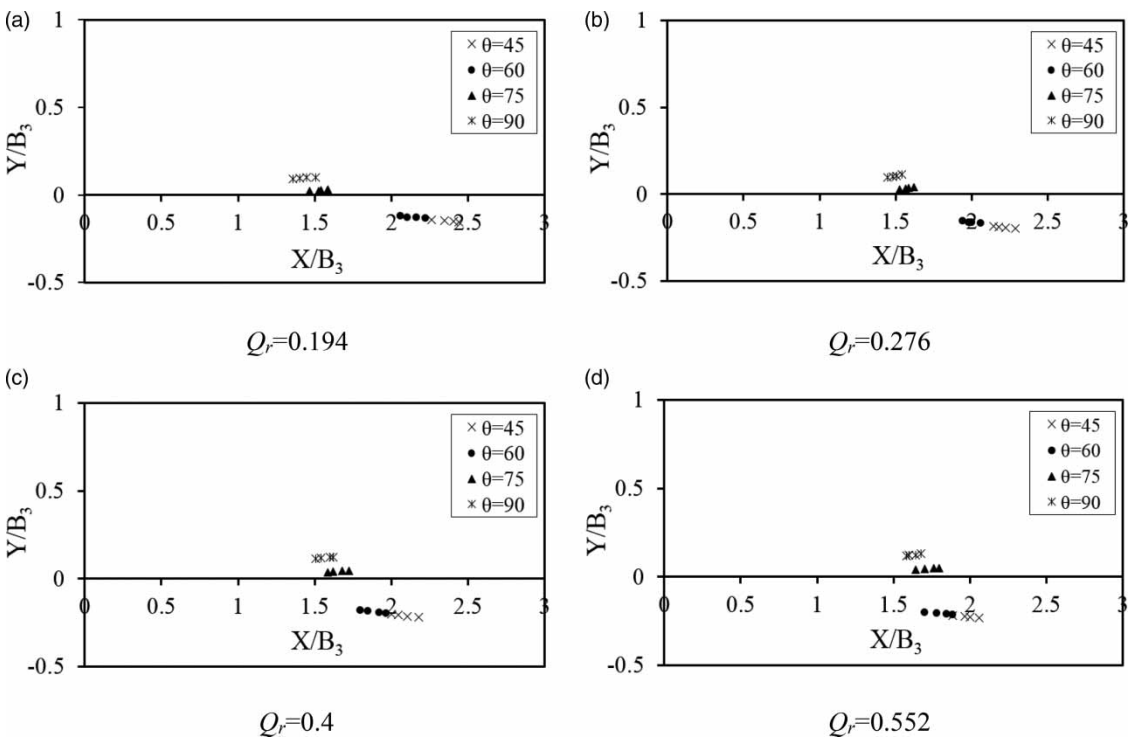

Figure 8 | Locations of four point bars corresponding to four Fr_{g3}.

which leads to the formation of point bars at a farther distance from the beginning of the post-confluence channel.

CONCLUSION

In this study, 64 experiments were conducted in a laboratory setup comprising two flumes with a confluence angle ($\alpha = 90^\circ$). The effects of three variables consisting of the bank slope angle of the main channel (θ), the discharge ratio of the tributary channel (Q_r) and the densimetric Froude number (Fr_{g3}) on both scouring at the confluence and sediment deposition in the post-confluence channel were experimentally investigated. The following conclusions were drawn. (1) When the minor discharge ratio is established at a confluence, the maximum effect of the bank inclination on scour depth is observed. Additionally, the mildest inclination angle ($\theta = 45^\circ$ in the current study) causes the minimum scour depth for a given densimetric Froude number. (2) For a given tributary flow at the confluence, the increase of densimetric Froude number in the post-confluence channel increases the maximum scour depth and decreases the height of the point bar. (3) Comparing the exponents of θ in the two obtained relationships (Equations (9) and (10)), it is concluded that the effect of bank slope angle on the height of the point bar is more than its effect on the scour depth. (4) Using the mildest inclination angle causes the formation of the point bar on the sloping bank and farther from the confluence in the downstream direction. Contrariwise, the steeper the inclination angle, the closer is the location of maximum point bar to the confluence. In the present study, the experiment using $\theta = 45^\circ$ and $Q_r = 0.194$ showed the best performance and reduced the maximum scour depth by 46%. (5) Generally, Fr_{g3} and θ demonstrated the most influence on the scour depth (d_{se}) and the height of the point bar (H_{se}), respectively. For future studies, it is suggested that the effect of change in bank slope angle be investigated simultaneously in both the main and tributary channels.

DATA AVAILABILITY STATEMENT

All relevant data are included in the paper or its Supplementary Information.

REFERENCES

Amini, N., Balouchi, B. & Shafai-Bajestan, M. 2017 Reduction of local scour at river confluences using a collar. *International Journal of Sediment Research* **32** (3), 364–372.

Best, J. L. 1987 Flow dynamics at river channel confluences: implications for sediment transport and bed morphology. In: *Recent Developments in Fluvial Sedimentology* (F. G. Ethridge, R. M. Flores & M. D. Harvey, eds), Special Publication 39, SEPM Society for Sedimentary Geology, Broken Arrow, OK, USA, pp. 27–35.

Best, J. L. 1988 Sediment transport and bed morphology at river confluences. *Sedimentology* **35** (3), 481–498.

Best, J. L. & Reid, I. 1984 Separation zone at open-channel junctions. *Journal of Hydraulic Engineering* **110** (11), 1588–1594.

Biron, P. M., Richer, A., Kirkbride, A. D., Roy, A. G. & Han, S. 2002 Spatial patterns of water surface topography at a river confluence. *Earth Surface Processes and Landforms* **27** (9), 913–928.

Biron, P. M., Ramamurthy, A. S. & Han, S. 2004 Three-dimensional numerical modeling of mixing at river confluences. *Journal of Hydraulic Engineering* **130** (3), 243–253.

Borghei, S. M. & Jabbari-Sahebari, A. 2010 Local scour at open-channel junctions. *Journal of Hydraulic Research* **48** (4), 538–542.

Boyer, C., Roy, A. G. & Best, J. L. 2006 Dynamics of a river channel confluence with discordant beds: flow turbulence, bed load sediment transport, and bed morphology. *Journal of Geophysical Research* **111**, F04007.

Bryan, R. B. & Kuhn, N. J. 2002 Hydraulic conditions in experimental rill confluences and scour in erodible soils. *Water Resources Research* **38** (5), 21.

Debnath, J., Das-Pan, N., Sharma, R. & Ahmed, I. 2019 Impact of confluence on hydrological and morphological characters of the trunk stream, a study on the Manu River of North-east India. *Environmental Earth Sciences* **78**, 190.

Geberemariam, T. K. 2016 Numerical analysis of stormwater flow conditions and separation zone at open-channel junctions. *Journal of Irrigation and Drainage Engineering* **143** (1), 05016009.

Ghobadian, R. & Shafai-Bajestan, M. 2007 Investigation of sediment patterns at river confluence. *Journal of Applied Sciences* **7** (10), 1372–1380.

Gong, Z., Zhang, C. K., Zuo, C. B. & Wu, W. D. 2011 Sediment transport following water transfer from Yangtze River to Taihu Basin. *Water Science and Engineering* **4** (4), 431–444.

Gurram, S. K., Karki, K. S. & Hager, W. H. 1997 Subcritical junction flow. *Journal of Hydraulic Engineering* **123** (5), 447–455.

Hager, W. H. 1989 Transitional flow in channel junctions. *Journal of Hydraulic Engineering* **115** (2), 243–259.

Hsu, C. C., Lee, W. J. & Chang, C. H. 1998 Subcritical open-channel junction flow. *Journal of Hydraulic Engineering* **124** (8), 847–855.

Khosravinia, P., Nikpour, M. R., Malekpour, A. & Hosseinzadeh Dalir, A. 2019 Effect of side slope of main channels on formation and penetration of scour hole in confluences. *River Research and Applications* **35**, 159–168.

Liu, T. H., Chen, L. & Fan, B. L. 2012 Experimental study on flow pattern and sediment transportation at a 90° open-channel confluence. *International Journal of Sediment Research* **27**, 178–187.

Melville, B. W. & Sutherland, A. J. 1988 Design method for local scour at bridge piers. *Journal of Hydraulic Engineering* **114** (10), 1210–1226.

Mohamadi, S., Shafai-Bajestan, M. & Ghobadian, R. 2013 Local scour at curved edge of open-channel junctions. *Caspian Journal of Applied Sciences Research* **2** (4), 33–40.

Mosley, M. P. 1976 An experimental study of channel confluences. *Journal of Geology* **84** (5), 535–562.

Nazari-Giglou, A., Jabbari-Sahebari, A., Shakibaeinia, A. & Borghei, S. M. 2016 An experimental study of sediment transport in channel confluences. *International Journal of Sediment Research* **31** (1), 87–96.

Rhoads, B. L. & Kenworthy, S. T. 1998 Time-averaged flow structure in the central region of a stream confluence. *Earth Surface Processes and Landforms* **23** (2), 171–191.

Rhoads, B. L. & Sukhodolov, A. N. 2008 Lateral momentum flux and the spatial evolution of flow within a confluence mixing interface. *Water Resources Research* **44**, W08440.

Roy, A. G., Roy, R. & Bergeron, N. 1988 Hydraulic geometry and changes in flow velocity at a river confluence with coarse bed material. *Earth Surface Processes and Landforms* **13** (7), 583–598.

Seyedian, S. M., Shafai-Bajestan, M. & Farasati, M. 2014 Effect of bank slope on the flow patterns in river intakes. *Journal of Hydrodynamics* **26** (3), 482–492.

Shakibainia, A., Tabatabai, M. R. M. & Zarrati, A. R. 2010 Three-dimensional numerical study of flow structure in channel confluences. *Canadian Journal of Civil Engineering* **37** (5), 772–781.

Sharifipour, M., Bonakdari, H., Zaji, A. H. & Shamshirband, S. 2015 Numerical investigation of flow field and flowmeter accuracy in open-channel junctions. *Engineering Applications of Computational Fluid Mechanics* **9** (1), 280–290.

Weber, L. J., Schumate, E. D. & Mawer, N. 2001 Experiments on flow at a 90° open-channel junction. *Journal of Hydraulic Engineering* **127** (5), 340–350.

Wuppukondur, A. & Chandra, V. 2017 Methods to control bed erosion at 90° river confluence: an experimental study. *International Journal of River Basin Management* **15** (3), 297–307.

Yuan, S., Tang, H., Xiao, Y., Qiu, X. & Xia, Y. 2017 Water flow and sediment transport at open-channel confluences: an experimental study. *Journal of Hydraulic Research* **56** (3), 333–350.

Zhang, T., Xu, W. & Wu, C. 2009 Effect of discharge ratio on flow characteristics in 90° equal-width open-channel junction. *Journal of Hydrodynamics* **21** (4), 541–549.

First received 27 March 2020; accepted in revised form 11 June 2020. Available online 24 June 2020